Chest electrical impedance tomography examination, data analysis, terminology, clinical use and recommendations: consensus statement of the TRanslational EIT developmeNt stuDy group

Inéz Frerichs, Marcelo B. P. Amato, Anton H. van Kaam, David G. Tingay, Zhanqi Zhao, Bartłomiej Grychtol, Marc Bodenstein, Hervé Gagnon, Stephan H. Böhm, Eckhard Teschner, Ola Stenqvist, Tommaso Mauri, Vinicius Torsani, Luigi Camporota, Andreas Schibler, Gerhard K. Wolf, Diederik Gommers, Steffen Leonhardt, Andy Adler, TREND study group

ONLINE SUPPLEMENT 3

EIT waveforms and regions-of-interest

EIT waveforms and regions-of-interest

This electronic online supplement (EOS 3) describes how EIT waveforms are generated from raw EIT images and how they are affected by the main physiological processes in the chest. The most common regions of interest (ROI) used to quantitatively analyze EIT regional phenomena are explained, followed by the filtering procedures useful for the analysis of EIT waveforms. Finally, we address the issues of noise and other interferences impacting EIT waveforms. Figure E3.1 shows the sequences of all processes involved in EIT examinations and EIT data analysis and the place of this EOS in the sequence.
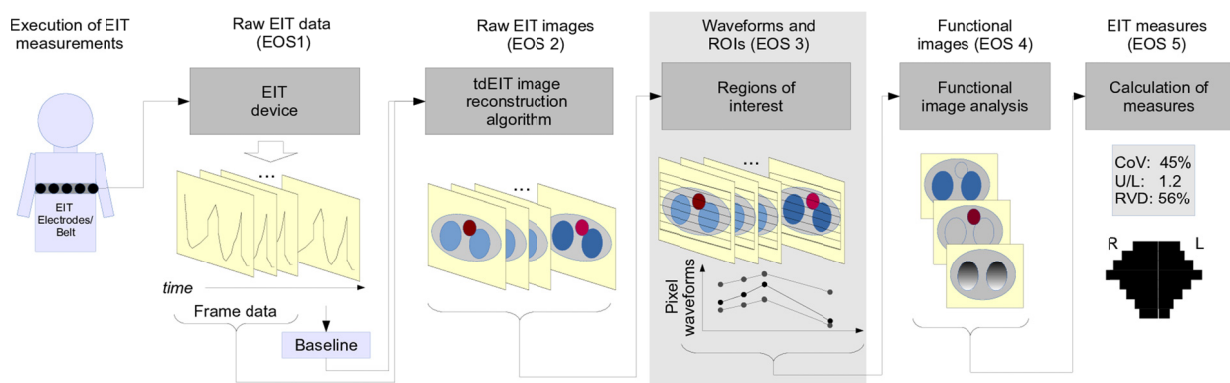

Figure E3.1. Sequence of processes involved in EIT chest examination and data analysis. EOS 3 (gray background) describes the EIT waveforms and regions of interest (ROI). Abbreviations: EOS, electronic online supplement; tdEIT, time-difference EIT; ROI, region-of-interest; CoV, center of ventilation; U/L, upper-to-lower ventilation ratio; RVD, regional ventilation delay; R, right; L, left.

EIT waveforms

An EIT waveform is a sequence of impedance change values as a function of time, generated online or offline, from a time series of raw EIT images. EIT waveforms can be global or regional. The global impedance waveform is based on the sum or average of impedance changes of all image pixels, while regional impedance waveforms are the sums or averages of relative impedance changes within defined ROIs. Pixel waveforms originate from the smallest "ROI", a single image pixel.

EIT waveforms consist of different periodic and non-periodic signals of multiple origins (Figure E3.2). Periodic (or quasiperiodic) signals are related to mechanical and spontaneous ventilation and cardiac action, as well as interferences from some medical

devices, such as pulsating air suspension mattresses and pacemakers. Non-periodic signals may be caused by spontaneous or ventilator-induced ventilation maneuvers, or can result from interferences such as body movements, changes of contact impedance over time, or baseline changes due to EIT hardware drift.
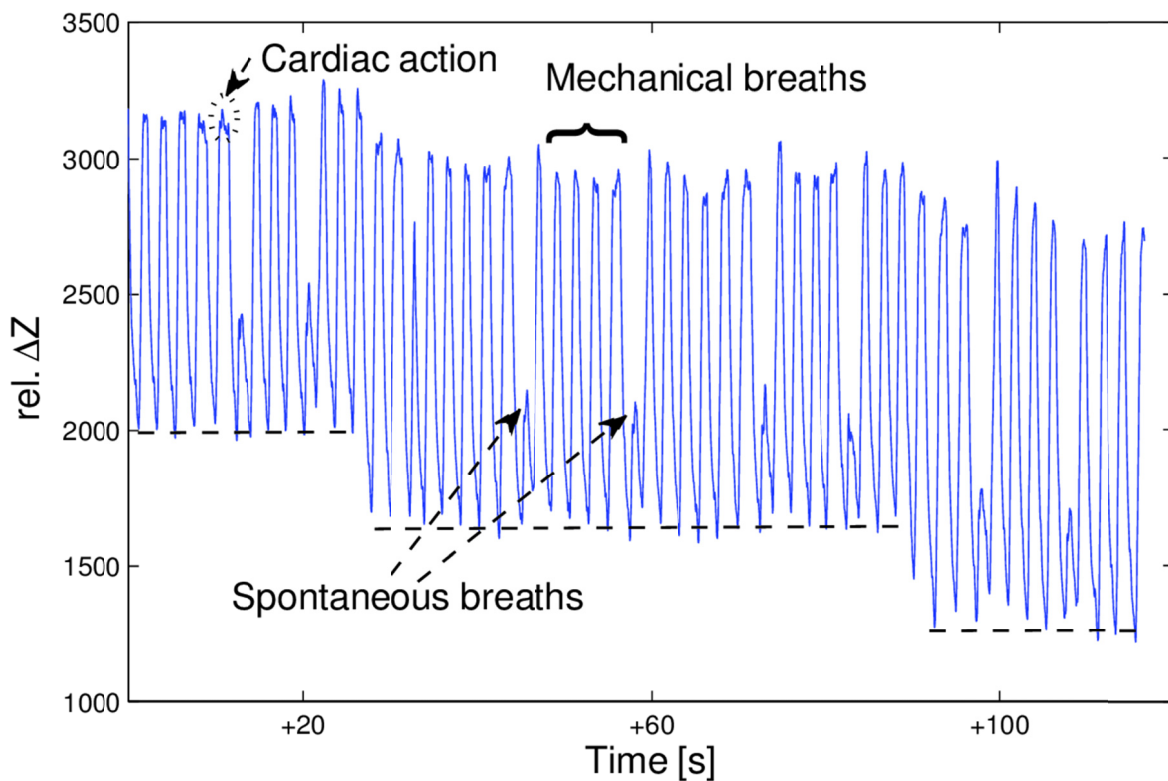
Figure E3.2. Example of a global impedance waveform containing periodic and non-periodic signals during a decremental positive end-expiratory pressure (PEEP) trial in a mechanically ventilated patient with ARDS. (The data was acquired using the PulmoVista 500 device (Dräger Medical, Lübeck, Germany).) Impedance changes induced by ventilation are larger than those induced by cardiac activity. The latter can be discerned at the end-inspiratory peaks of the EIT signal. Dashed lines at end-expiratory lung impedance values at three decremental PEEP levels highlight the stepwise fall in end-expiratory volume. rel. ΔZ, relative impedance change.

Regions of interest

A region of interest (ROI) is a selected subset of an image identified for a particular purpose. In EIT images, ROIs have been chosen to group the image pixels which represent regional physiological aspects. The EIT waveform in a ROI is the sum or average of the pixel waveforms for all pixels in the ROI. Since EIT waveforms contain regional information from various sources, it is necessary to isolate the different components of EIT signals to

quantitatively analyze the images using relevant EIT measures (EOS 5). By the definition of the ROI, image pixels are chosen to reflect the regional changes associated with relevant physiological or pathological effects. The other approach to isolate regional information from the images is filtering, discussed in the section "Frequency filtering" later in this EOS.

In the most common case, ROIs are defined to assess regional ventilation. For example, ROIs of horizontal layers are appropriate for monitoring ventilation-related pathology which affects both lungs equally, and for assessing dependent vs. non-dependent lung behavior. ROIs that separate the left and right lungs are suitable for monitoring pathology likely to affect each lung differently. ROIs can also be defined to assess cardiac-related impedance changes. The anatomical location of breathing and heart beat-related impedance changes has been validated to correspond to the correct anatomical locations, when using anatomically accurate reconstruction algorithms (1).

- **Geometrical ROIs**

The simplest ROIs are defined geometrically as equal horizontal and/or vertical divisions of the image region, as illustrated in figure E3.3 (top row). Such regions are defined by horizontal and vertical slices which divide the image region into equally sized rectangles.

In cases where the physiology of interest is distributed in the anteroposterior direction, ROIs divide the image region with horizontal divisions. The minimum is a division into two regions, the anterior and the posterior (i.e., the upper and the lower in supine subjects). This approach has been used to calculate the ratio of anterior-to-posterior (i.e., upper-to-lower ventilation ratio) (2, 3), a measure originally called the "impedance ratio" (4) (see also EOS 5). The image region may be further divided into smaller ROIs if necessary (5-7). The maximum number of horizontal ROIs is the image resolution, where each horizontal ROI is a pixel height (typically 32 pixels for most common reconstruction algorithms) (8-10). This maximum vertical resolution increases the sensitivity of EIT data analysis for ventilation distribution monitoring (11). In figure E3.3, a division into two regions and into a larger numbers of regions is shown.

A further division of ROIs is to consider the left/right division between image regions (3, 12). Another common type of ROIs is generated by dividing the image regions into four quadrants (13).

There are a few drawbacks of horizontal ROIs defined on the global image. First, given the variability in thorax shape and the position of lungs within it, it is common that the most dependent ROIs contain only a small or no lung region. This is especially likely in obese patients where there is a larger layer of tissue surrounding the lungs. In this case, no

ventilation signal will be present in these dependent ROIs. The low signals in dependent ROIs can also be caused by lung collapse in these regions. One way to address this issue is to define the geometrical ROIs not within the whole image but only in a ROI representing the lungs (see the section "Lung ROIs" below). In this case, the lung ROI is first detected, and then horizontal or vertical geometrical divisions are identified in that region (14). In Figure E3.3, the top row shows the global image region and its subdivisions, while the bottom row shows subdivisions of the lung ROI.
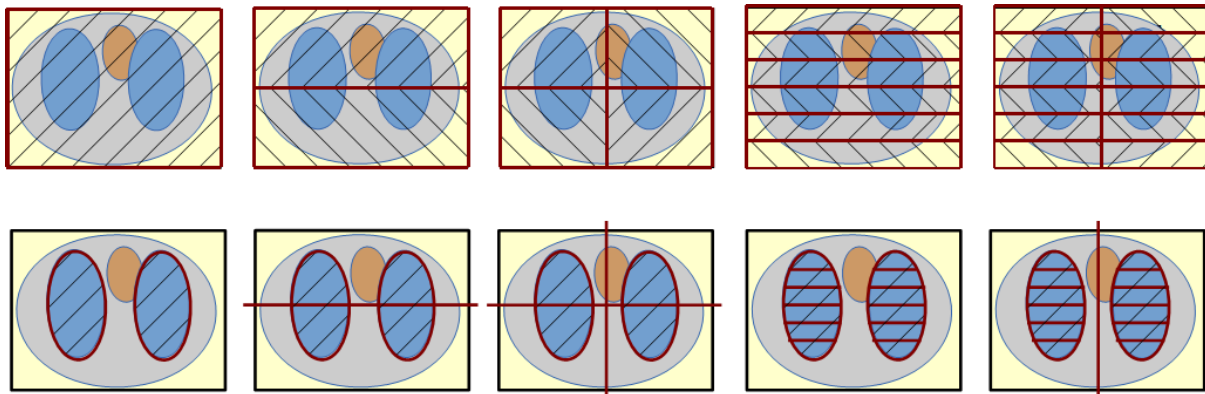

Figure E3.3. Different types of ROIs used to characterize the distribution of ventilation. The top row shows ROIs for the global image, while the bottom row illustrates ROIs for the division of the lung region only. From left to right: 1) global region, 2) anterior (upper) and posterior (lower) regions, 3) image quadrants (anterior right, anterior left, posterior right, posterior left), 4) multiple layers (six illustrated), and 5) multiple layers with left/right division. (Areas with oblique lines are contained within the respective ROIs.)

- **Lung ROIs**

As discussed above, some EIT image analysis methods require the identification of the lung regions (14-19). Most of the lung ROI identification methods identify lungs as regions with large values in functional EIT images (see also EOS 4). In these methods, the lung is the region in which fEIT image values are above a threshold, defined as a fraction of the maximum image value. Use of a smaller threshold increases the ROI size. It makes the identification of lung regions more complete, however, some nearby non-lung regions are detected as well. A larger threshold has the opposite effect. It better rejects the non-lung regions, but it is less able to detect all lung regions. Pulletz et al. and Becher et al. analyzed the influence of threshold settings for this purpose (11, 20). The definition of the ROI using a threshold of 20–35% of the maximum pixel values was recommended. Higher threshold values have been shown to obscure the differences in the degree of ventilation homogeneity

between ARDS patients and patients with healthy lungs (20). The impact of the type of functional images used to generate the lung ROIs on the quantitative analysis of ventilation distribution was also examined (21). Dynamic determination of threshold values is also possible (22). However, there is no optimal threshold value that can separate lung regions from other thoracic tissues.
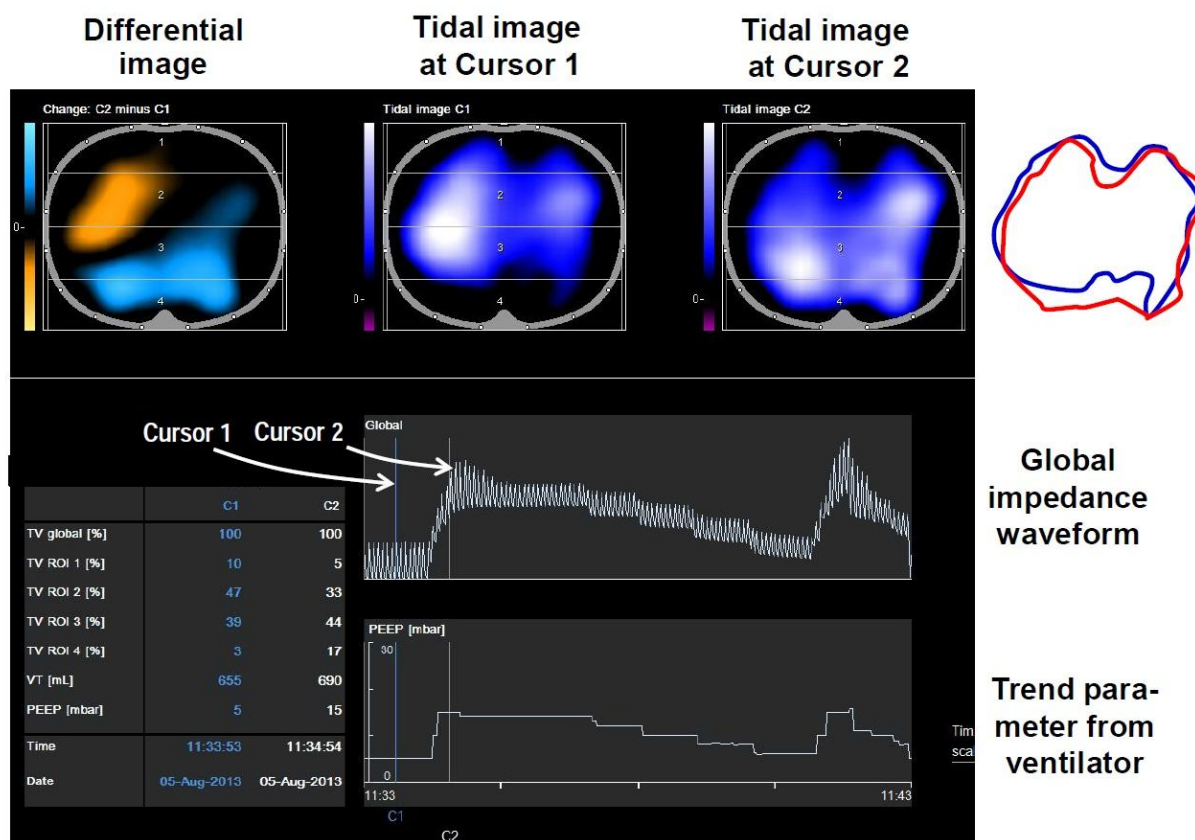
Figure E3.4. EIT examination of an anesthetized supine patient ventilated at different end-expiratory pressure (PEEP) values using the PulmoVista 500 device (Dräger Medical, Lübeck, Germany). The two tidal images (top right) show the ventilation distribution at PEEP of 5 and 15 cmH$_2$O, the differential image (top left) highlights the loss (orange) and gain (blue) in regional ventilation between these two time points (cursor 1 and cursor 2). The lung ROIs identified from the two tidal images are plotted as blue (PEEP 5 cmH$_2$O) and red (PEEP 15 cmH$_2$O) lung contours at the right top edge of the figure. Note that the ventral and dorsal boundaries at PEEP 5 are positioned above the corresponding PEEP 15 boundaries.

A further issue that needs to be taken into account when lung ROI is defined is that the ventilation distribution depends on the ventilator setting, for instance the end-expiratory pressure (PEEP). At low PEEP, ventilation occurs mainly in non-dependent regions, and at

high PEEP levels, ventilation shifts toward dependent regions (Figure E3.4). Thus, to approximate the total lung area, it is useful to combine the regions identified at low and at high PEEP. However, this solution is still unable to identify collapsed lung regions. To identify such non-ventilated lung tissue, some other approaches have been developed. Mirroring the lung areas from one side to the other will include collapsed regions which are present in one lung but not the other (23). Since perfusion may still be present in collapsed lung tissue, ROI definitions from the EIT perfusion signal may be added to the ventilation-defined lung ROI (24). Given that lung size in healthy adults depends on the height (25) and weight, (26) built a database of lung sizes and locations in EIT images from CT images and correlated them with height and weight measurements. Using this database, it is possible to estimate the lung ROI and thorax shape in an image from a patient's height and weight.

The heart region is more difficult to identify than the lungs because the cardiac-related signals are smaller, and there are cardiac-frequency contributions throughout the image. This means that a simple frequency filter will identify a larger region than the heart. Several more sophisticated techniques have been proposed (1, 16, 23, 27, 28). ROIs have been identified with ECG gating (29, 30) or principal component analysis (24, 31), and separate the heart area and the perfused lung tissue region. A common approach used by many of these techniques is an initial identification of the lung ROI, and then the use of this region to exclude areas which would otherwise be identified by cardiac-frequency filtering.

- **Examples of ROIs and associated waveforms**

Three typical ROI definitions for regional lung ventilation and their associated waveforms are illustrated in figure E3.5. In this example, a linear regression functional EIT image (fEIT) is shown, where colors are normalized to the maximum image value. Two divisions of the global fEIT image are shown. Figure E3.5 (left) shows four quadrants. Figure E3.5 (right) shows four anteroposterior layers with equal height. A lung ROI is shown (Figure E3.5, middle). Here the lung region is defined as those pixels with values above a threshold of 20% of the maximum.
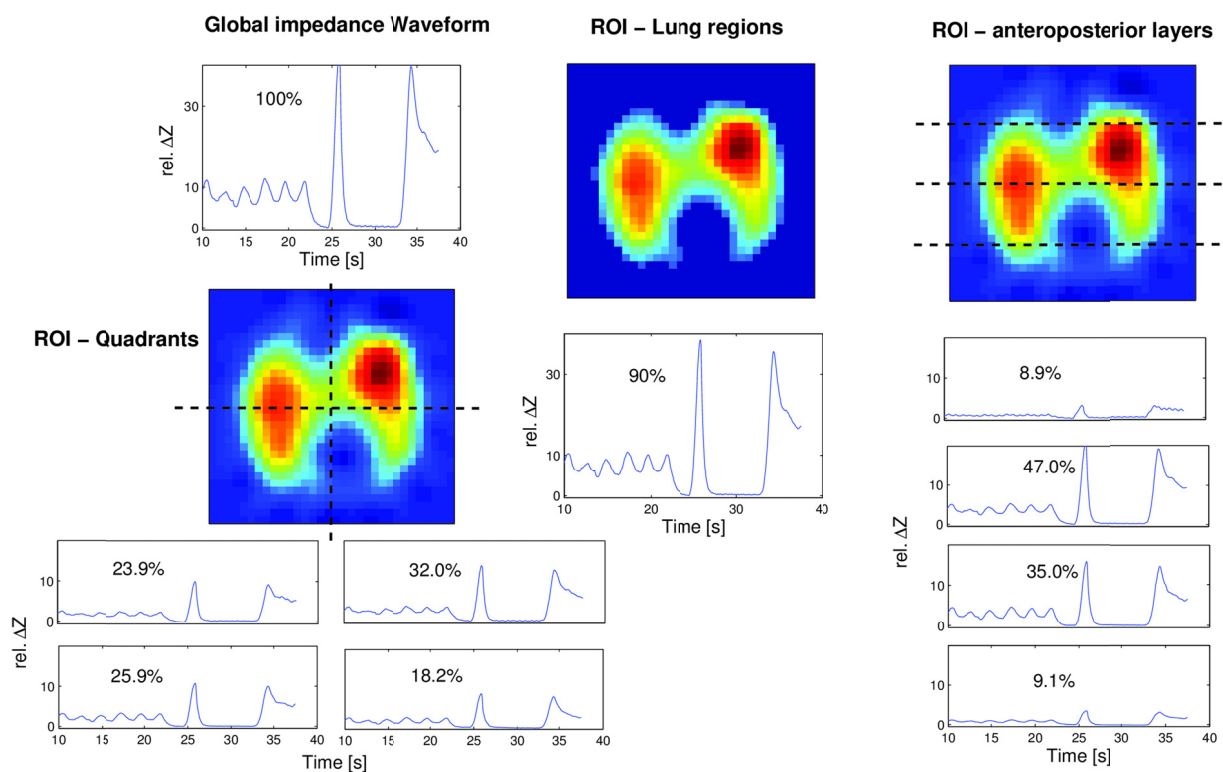
Figure E3.5. Commonly used regions of interest (ROIs) defined in an fEIT image of a healthy volunteer during pulmonary function testing. (The raw data was acquired with the Goe-MF II device (CareFusion, Höchberg, Germany).) ROIs from left to right are four quadrants, lung regions with a threshold of 20% of maximum image value, four anteroposterior layers with equal heights. The global impedance waveform (left top) is normalized to 100%. Regional impedance waveforms and percentages represent impedance changes within the corresponding ROIs during the forced maneuver. rel. ΔZ, relative impedance changes.

EIT scan rate

- **Available scan rates from typical EIT equipment**

Modern medical EIT equipment offers a scan rate from 10-50 scans per second. Some systems offer much faster rates, including an industrial system with a frame rate up to 1000 frames per second (32). Increasing the scan rate increases the temporal resolution, and means that transient phenomena can be better resolved. Since a higher scan rate means that each measurement must be made more quickly, higher rates may also cause a reduction in the signal quality. For applications of prolonged monitoring, recording EIT data at high scan rates also results in large data files.

- **Scan rate requirements for typical monitoring tasks**

The EIT scan rate requirements depend on the frequency of the signal components to be analyzed. Respiratory frequency in adults and children is usually lower than 40 breaths per minute (~0.67 Hz). Assuming a heart rate lower than 180 beats per minute (3 Hz), then, according to the Nyquist–Shannon sampling theorem, a scan rate above 6 frames per second should be sufficient for the sampling and separation of the respiratory and cardiac-related signals. In practice, such as scan rate is far too low. First, there are important features in the cardiac activity within each beat, which should be resolved. Furthermore, classical sampling theory is not directly applicable, since EIT samples both in space and time (measurements in an EIT scan are made sequentially (33)). The effect is to increase the required sampling rate to avoid aliasing (34).
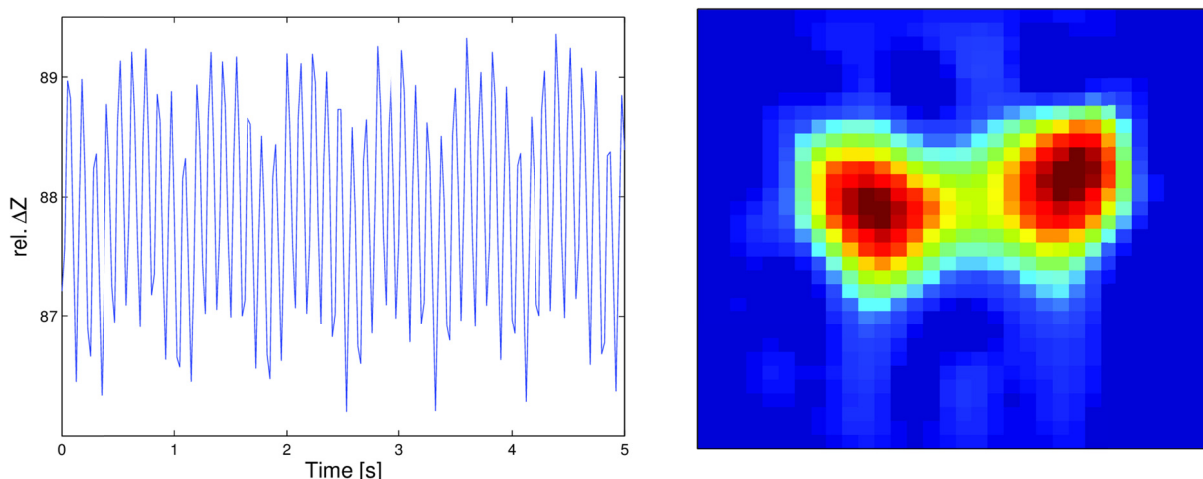
Figure E3.6. Global impedance waveform (left) and fEIT image (right) acquired by the PulmoVista 500 EIT device (Dräger Medical, Lübeck, Germany) in an anesthetized supine pig during high-frequency oscillatory ventilation. The oscillatory ventilation rate was 9 Hz and EIT scan rate 40 Hz. Slower periodic impedance changes in the global waveform represent the cardiac-related signal (the heart rate was 1.3 Hz). rel. ΔZ, relative impedance change.

Thus, in practice, higher scan rates are recommended, in order to capture the higher frequency details of these EIT signals. The respiratory and heart rate may vary dramatically because lung ventilation and heart action are not strictly periodic. Additionally, diseased lungs may have slow and fast compartments (35) and thus be ventilated inhomogeneously. These effects increase the scan rate requirements for respiratory and cardiac-related signals. We recommend a scan rate above 10 Hz for analyzing ventilation-related impedance

changes and 25 Hz for cardiac-related impedance changes. For high frequency oscillatory ventilation, which contributes much higher frequency signals, the scan rate of EIT should correspondingly larger (Figure E3.6). High scan rates are also needed for the assessment of rapid gas volume changes at high air-flow rates (35-41).

Frequency filtering

- **Definition and application**

Cardiac action and ventilation occur at different rates in humans, and their EIT signals components can thus be discriminated using frequency filtering (29, 42, 43). The breathing rate (12 -16 breaths/min in a spontaneously breathing adult) is typically much lower than cardiac rate (60 – 90 beats/min). It is therefore possible to design a digital filter to separate the ventilation and cardiac activity components provided by EIT. In the simplest case, a low-pass filter (which lets low-frequency components of a signal "pass" through while removing higher frequencies) identifies the ventilation signal while a high-pass filter with an opposite effect identifies cardiac-related information. In practice, however, a band-pass filter (which lets a range of frequencies pass while removing higher and lower frequencies) is used. It removes some low-frequency disturbances (e.g. baseline drift related to hardware or drying of the electrode gel) as well as high-frequency error sources (e.g. other interfering electrical equipment). The band-pass filters can be generated by defining the expected normal frequency ranges for breathing and cardiac activity. Other band-pass filters are designed centered around a single frequency with an appropriate bandwidth. The center frequency of the filter may be obtained directly from the ventilator or ECG monitor, from a human operator analyzing the signal spectrum or from an automated algorithm that identifies the highest peaks from the frequency spectrum (corresponding to the first harmonics) in the frequency ranges expected for ventilation or cardiac activity.

Digital filtering can be performed in two ways. The raw EIT data can be filtered, and then reconstructed, or the pixel waveforms in a sequence of raw EIT images can be filtered. The results of both of these operations are identical when the reconstruction algorithm is linear, which is the case for most of the commonly used reconstruction algorithms for chest imaging. The digital filters can be implemented either in the time or frequency domains. The design of digital filters is beyond the scope of this document, but many textbooks and software toolboxes are available to assist in their design. In the design of digital filters, there are several issues, such aliasing and the effects of scan time and non-periodic signals, that can contribute undesired effects. They are discussed in the following paragraphs.

Other techniques such as ECG-gated EIT acquisition (17) and principal component analysis (PCA) (24) have been proposed to circumvent some of the limitations observed with frequency filtering. Some papers combine one of these two techniques with frequency filtering to achieve better separation of the ventilation and cardiac activities (24). ECG-gating can be performed at the hardware level where a series of EIT measurements are automatically triggered whenever a QRS complex is detected in the patient's ECG. When the ECG is acquired simultaneously and synchronized with the EIT measurements, ECG-gating can also be performed by post processing the acquired EIT data to identifying those EIT frames where a QRS complex was synchronously detected in the ECG. Ensemble averaging can then be performed on ECG-gated EIT measurements to improve the signal-to-noise ratio (SNR) of the cardiac-related information from the EIT measurement. The same gating process can also be performed using the ventilator trigger instead of the QRS complex in order to increase the SNR of the ventilation-related information.

- **Aliasing**

The most important signal processing issue to consider when using digital frequency filtering is aliasing. Aliasing is a signal artefact in which content at one frequency in the original data is represented at a different frequency in the filter output. It occurs when the sampling frequency is not high enough for the frequency content of the signal. According to the Nyquist-Shannon sampling theorem, aliasing occurs when the sampling rate is less than twice the maximum frequency component of the signal. One special worry is that frequency components near the sampling frequency can appear via aliasing as low frequency artefacts in the image. As mentioned, EIT has a mix of spatial and temporal aliasing which is more complicated than that described by the Nyquist-Shannon theory (33, 34). Extra care should be taken when the heart rate is an exact multiple of the ventilation rate (or the vice versa, with high-frequency ventilation) which could occur for instance if ventilation occurs in neonates at e.g. 40 breaths/min and a heart rate of 120 beats/min. The cardiac frequency would then be contaminated with the third harmonic of the ventilation making it impossible to discriminate between them with frequency filtering alone.

- **Inadequate sample time**

Unlike the sampling frequency, a parameter that is sometimes neglected in design of data acquisition is the duration of sample acquisition, or sample time (T). In cases where data are acquired only for a very short sample time, it is impossible to discriminate between close adjacent frequencies, and they will appear superposed in the spectrum. The frequency

resolution, or the difference between adjacent frequency bins, is given by the inverse of the sample time, $1/T$. The frequency resolution is also the lowest frequency difference that is distinguishable in the signal. For example, if 30 seconds of EIT data are acquired, it will not be possible to distinguish frequencies which differ by 1/30 s (2 per minute), making ventilation frequencies of 6 and 8 breaths per minute appear identical.

- **Non-periodic changes**

Frequency filtering works well in simple cases where the respiratory and heart rates are well separated and do not vary during the whole acquisition time (in the signal processing literature, this is referred to as a "stationary" signal). A mechanically ventilated patient with a constant tidal volume (V_T) and breathing rate can be considered a stationary EIT signal source, assuming the heart rate was also relatively constant over the period of time. During spontaneous breathing, the breathing rate can greatly vary and including pauses in breathing (e.g. sleep apnea). The heart rate might also vary, especially if the subject is performing tasks which include exercise. In such cases, an adaptive filtering strategy would be recommended, in which filters adapt over time to best match the frequencies of the heart and breathing activity.

Other (patho-)physiological events that may be visible in EIT data, such as dynamic hyperinflation, produce non-periodic changes of impedance that might be missed if high-pass frequency filtering alone is used, since it typically removes very slow changes. This is true also of changes in ventilator settings, such as PEEP or V_T. Slow changes of the EIT signal can also occur due to hardware electronic drift, drying of the electrode gel or patient movement (resulting in posture or electrode position changes). Although these slow impedance changes are often not clinically relevant, it might be difficult in some cases to distinguish them from those occurring from physiological events such as the onset of atelectasis or pulmonary edema.

Description of expected waveforms

- **Ventilation-related changes in EIT waveforms**

The shape of EIT waveforms is altered by any frequency filtering applied to the signals. Commercially available EIT devices often set filters automatically to enhance visualization of ventilation waveform (i.e., by low-pass filtering).

In the case of a completely passive mechanically ventilated patient, ventilation impedance-time waveforms usually present a stable end-expiratory level. After an

impedance increase during inspiration, the ventilation waveform reaches a peak value, corresponding to end–inspiration. The waveform falls at end-expiration, and the impedance value typically reaches the previous end-expiratory level (Figure E3.7).

There is a close correlation between global and regional V_T and global and regional tidal impedance changes. If V_T does not change over time (e.g., during a volume-controlled mode), the shape and dimension of each ventilation waveform will be stable, and a small observation time would be enough to obtain clinically relevant information. On the other hand, during pressure-controlled ventilation, changes in the peak values of global and regional impedance waveforms could yield clinical information on changes of global or regional respiratory system compliance and/or airway resistance.
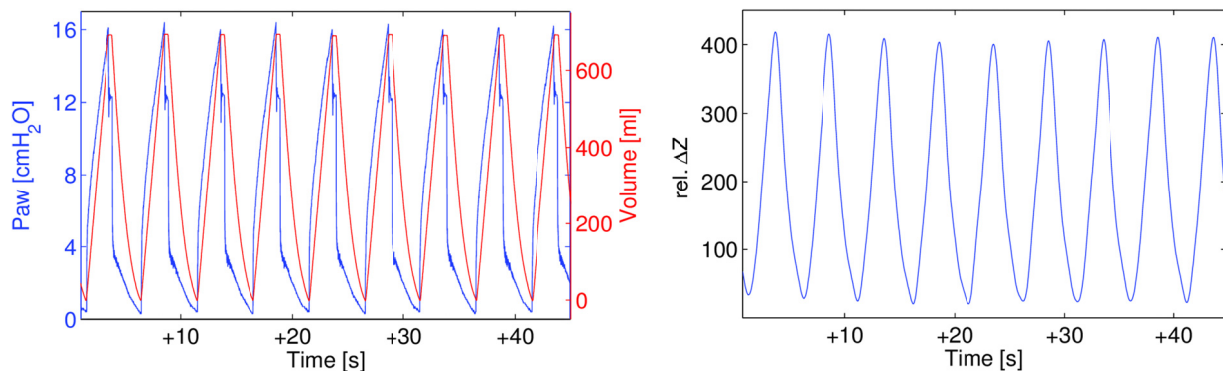
Figure E3.7. EIT waveform of a passive mechanically ventilated patient acquired with the PulmoVista 500 device (Dräger Medical, Lübeck, Germany). Left: Airway pressure (Paw) (blue) and volume (red) signals obtained from the ventilator during the examination. Right: global EIT waveform. Paw, airway pressure; rel. ΔZ, relative impedance change.

For spontaneously breathing patients (Figure E3.8), there is variability in the shape and magnitude of the ventilation EIT waveform. The baseline end-expiratory impedance level can vary over time, and variations of respiratory rate and respiratory muscle activity, can increase or decrease end-inspiratory lung volume and, consequently, impedance. While the shape of each deflection of the global and regional impedance waveforms appears similar to that in controlled ventilation, time intervals and peak values are irregular. In such cases, several minutes of observation might be needed to obtain stable and comprehensive information.
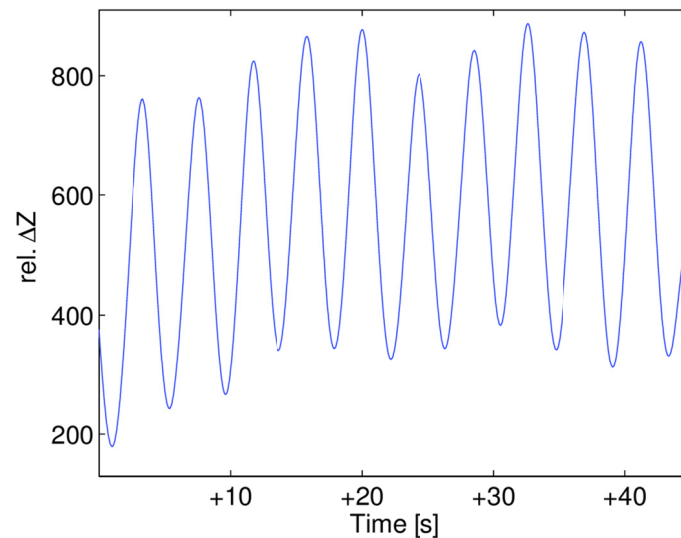
Figure E3.8. Global EIT waveform with ventilation-related changes in impedance obtained in a spontaneously breathing patient (PulmoVista 500, Dräger Medical, Lübeck, Germany). rel. ΔZ, relative impedance change.

In spontaneously breathing patients, inspiratory effort can vary over time due to a multitude of factors (e.g., ventilation support, arterial respiratory gas concentrations, anxiety, body temperature, etc.) and this can lead to variations in global and regional peak inspiratory and trough expiratory impedance values and, consequently, in the distribution of tidal impedance changes across the imaging field. Higher peak levels at end-inspiration represent higher air content, allowing monitoring of sighs or re-expansion of previously collapsed regions (i.e., after atelectasis or pneumothorax resolution).

- **Cardiac-related changes in EIT waveforms**

The EIT signal changes induced by cardiac activity are referred to as the pulsatility. The pulsatility component in EIT data is small compared to the ventilation signal and it is often identified by using frequency filtering. Typically, a band pass filter is applied which rejects the contributions at ventilation rate and it higher harmonics (Figure E3.9). The pulsatile EIT waveform is complicated because of the propagation of blood from the heart through the lung regions. During systole, blood from the right ventricle leaves the heart and moves into the lungs through the pulmonary arteries. This component of blood flow stays in the EIT field of view. Blood from the left ventricle moves through the aorta, and leaves the field of view of a thoracic EIT electrode placement. During systole, therefore, there is an impedance increase in the heart and an impedance decrease which propagates through the lungs (Figure E3.8, left). When the heart rate is high, the two deflections can be superimposed in the global signal and only one phase is evident, similar to that of ventilation. However,

regional waveform analysis can separate these two waveforms (Figure E3.9, middle and right).
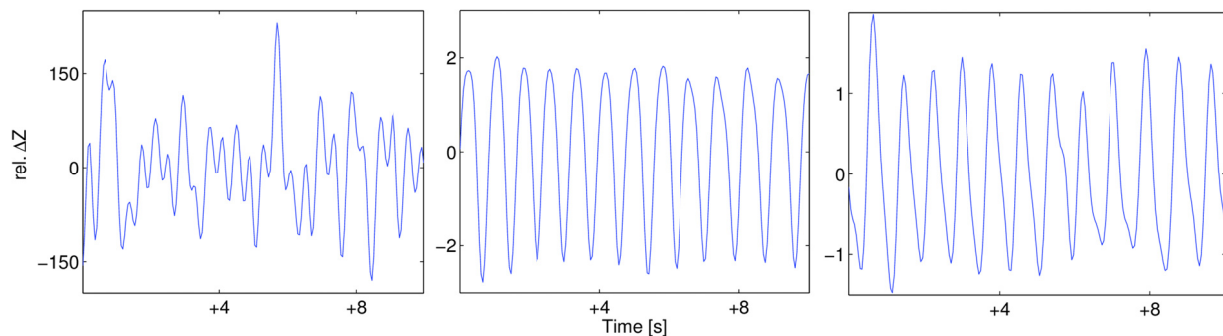
Figure E3.9. Pulsatile EIT waveforms. Left: global relative impedance waveform combining heart and pulmonary perfusion-related signals. Middle: regional impedance waveform of a single pixel in the heart region. Right: regional impedance waveform of a single pixel in the lung region. There is a phase shift between the two latter regional waveforms. rel. ΔZ, relative impedance change. (The EIT data was acquired using the PulmoVista 500 device (Dräger Medical, Lübeck, Germany).)

- **Origin of pulsatility in the EIT signal**

While the major contribution to the pulsatile EIT signal is blood perfusion, there are many sources affecting these signals (44). Pulsatile impedance changes are proportional to blood volume changes and not directly to the blood flow. For example, in the extreme case of constant blood flow or flow in a completely rigid vessel, there would be no impedance change (and thus no pulsatility) as volume in the vessel would be constant. In the opposite extreme, blood volume oscillation in a vessel closed by an occlusion (e.g., in the presence of an arterial blood clot) would give an impedance change over time in absence of flow. These extreme differences illustrate that pulsatile impedance originates in regional blood volume changes and is not a direct measure of lung perfusion. However, the EIT pulsatile signal in the lungs does have a major contribution from perfusion, since blood flow in the lungs affects the impedance distribution by cyclic expansion of pulmonary blood vessels and by inducing red blood cell alignment with the blood flow. Several *in vivo* studies could show good correlation between the pulsatile impedance waveform and perfusion (16, 28, 45, 46). Using frequency filtering and ROI analysis, Ferrario et al discriminated heart and lung regions in the thorax (1).

Common artifacts in EIT waveforms

While EIT signals contain much useful physiological information, there are many sources of artifacts which can corrupt the EIT waveforms. Artefacts can originate in the raw EIT data, or from the signal processing, where, for example, inappropriate filtering might cause superimposition of waveforms from different origins. A number of effects (such as body movement and posture change) can alter baseline end-expiratory impedance. As waveforms are usually calculated as relative changes to baseline, this will alter the magnitude and shape of the ventilation impedance waveforms.

Changes in electrode-skin contact impedance influence the calculated waveforms. The electrode-skin impedance is affected by the contact force, drying of the gel or contact fluid and other factors. EIT system vendors provide a measure of electrode-skin contact impedance as a measure of signal quality.

Possible interference with other medical devices must be taken into account in monitoring of intensive care patients, where electrical "noise" is produced by many other devices in the ICU. An overview of most common interferences encountered during EIT examinations in the ICU like pulsation therapy with air suspension mattresses, continuous cardiac output monitoring and impedance pneumography has been provided by Frerichs et al. along with the recommendations on EIT data analysis under these circumstances (47). Other devices emitting electromagnetic signals may potentially interfere with EIT measurements. However, overall, modern EIT devices are capable of generating high-quality data in the majority of experimental and clinical settings.

Document preparation

The first draft of this online document was prepared by Z. Zhao with collaboration of H. Gagnon, O. Stenqvist, T. Mauri, I. Frerichs and A. Adler. It was reviewed and approved by all other authors and collaborators.

References

1.   Ferrario D, Grychtol B, Adler A, Sola J, Bohm SH, Bodenstein M. Toward morphological thoracic eit: Major signal sources correspond to respective organ locations in CT. *IEEE Trans Biomed Eng* 2012;59:3000-3008.

2.   Rossi Fde S, Yagui AC, Haddad LB, Deutsch AD, Rebello CM. Electrical impedance tomography to evaluate air distribution prior to extubation in very-low-birth-weight infants: A feasibility study. *Clinics (Sao Paulo)* 2013;68:345-350.

3.   Schramel J, Nagel C, Auer U, Palm F, Aurich C, Moens Y. Distribution of ventilation in pregnant shetland ponies measured by electrical impedance tomography. *Respir Physiol Neurobiol* 2012;180:258-262.

4.   Kunst PW, Vazquez de Anda G, Bohm SH, Faes TJ, Lachmann B, Postmus PE, de Vries PM. Monitoring of recruitment and derecruitment by electrical impedance tomography in a model of acute lung injury. *Crit Care Med* 2000;28:3891-3895.

5.   Odenstedt H, Lindgren S, Olegard C, Erlandsson K, Lethvall S, Aneman A, Stenqvist O, Lundin S. Slow moderate pressure recruitment maneuver minimizes negative circulatory and lung mechanic side effects: Evaluation of recruitment maneuvers using electric impedance tomography. *Intensive Care Med* 2005;31:1706-1714.

6.   Meier T, Luepschen H, Karsten J, Leibecke T, Grossherr M, Gehring H, Leonhardt S. Assessment of regional lung recruitment and derecruitment during a PEEP trial based on electrical impedance tomography. *Intensive Care Med* 2008;34:543-550.

7.   Victorino JA, Borges JB, Okamoto VN, Matos GF, Tucci MR, Caramez MP, Tanaka H, Sipmann FS, Santos DC, Barbas CS, Carvalho CR, Amato MB. Imbalances in regional lung ventilation: A validation study on electrical impedance tomography. *Am J Respir Crit Care Med* 2004;169:791-800.

8.   Frerichs I, Dargaville PA, van Genderingen H, Morel DR, Rimensberger PC. Lung volume recruitment after surfactant administration modifies spatial distribution of ventilation. *Am J Respir Crit Care Med* 2006;174:772-779.

9.   Zick G, Elke G, Becher T, Schadler D, Pulletz S, Freitag-Wolf S, Weiler N, Frerichs I. Effect of PEEP and tidal volume on ventilation distribution and end-expiratory lung volume: A prospective experimental animal and pilot clinical study. *PLoS One* 2013;8:e72675.

10.   Tingay DG, Wallace MJ, Bhatia R, Schmolzer GM, Zahra VA, Dolan MJ, Hooper SB, Davis PG. Surfactant before the first inflation at birth improves spatial distribution of ventilation and reduces lung injury in preterm lambs. *J Appl Physiol* 2014;116:251-258.

11.   Pulletz S, van Genderingen HR, Schmitz G, Zick G, Schadler D, Scholz J, Weiler N, Frerichs I. Comparison of different methods to define regions of interest for evaluation of regional lung ventilation by EIT. *Physiol Meas* 2006;27:S115-127.

12.   Frerichs I, Hahn G, Hellige G. Gravity-dependent phenomena in lung ventilation determined by functional EIT. *Physiol Meas* 1996;17 Suppl 4A:A149-157.

13.   Muders T, Luepschen H, Zinserling J, Greschus S, Fimmers R, Guenther U, Buchwald M, Grigutsch D, Leonhardt S, Putensen C, Wrigge H. Tidal recruitment assessed by electrical impedance tomography and computed tomography in a porcine model of lung injury. *Crit Care Med* 2012;40:903-911.

14.   Frerichs I, Dargaville PA, Rimensberger PC. Regional respiratory inflation and deflation pressure-volume curves determined by electrical impedance tomography. *Physiol Meas* 2013;34:567-577.

15.   Elke G, Fuld MK, Halaweish AF, Grychtol B, Weiler N, Hoffman EA, Frerichs I. Quantification of ventilation distribution in regional lung injury by electrical impedance tomography and xenon computed tomography. *Physiol Meas* 2013;34:1303-1318.

16.   Schibler A, Pham TM, Moray AA, Stocker C. Ventilation and cardiac related impedance changes in children undergoing corrective open heart surgery. *Physiol Meas* 2013;34:1319-1327.

17.   Vonk Noordegraaf A, Kunst PW, Janse A, Marcus JT, Postmus PE, Faes TJ, de Vries PM. Pulmonary perfusion measured by means of electrical impedance tomography. *Physiol Meas* 1998;19:263-273.

18.   Zhao Z, Moller K, Steinmann D, Frerichs I, Guttmann J. Evaluation of an electrical impedance tomography-based global inhomogeneity index for pulmonary ventilation distribution. *Intensive Care Med* 2009;35:1900-1906.

19.   Becher TH, Bui S, Zick G, Blaser D, Schadler D, Weiler N, Frerichs I. Assessment of respiratory system compliance with electrical impedance tomography using a positive end-expiratory pressure wave maneuver during pressure support ventilation: A pilot clinical study. *Crit Care* 2014;18:679.

20.   Becher T, Vogt B, Kott M, Schadler D, Weiler N, Frerichs I. Functional regions of interest in electrical impedance tomography: A secondary analysis of two clinical studies. *PLoS One* 2016;11:e0152267.

21.   Pulletz S, Elke G, Zick G, Schadler D, Scholz J, Weiler N, Frerichs I. Performance of electrical impedance tomography in detecting regional tidal volumes during one-lung ventilation. *Acta Anaesthesiol Scand* 2008;52:1131-1139.

22.   Gomez-Laberge C, Arnold JH, Wolf GK. A unified approach for EIT imaging of regional overdistension and atelectasis in acute lung injury. *IEEE Trans Med Imaging* 2012;31:834-842.

23.   Zhao Z, Steinmann D, Muller-Zivkovic D, Martin J, Frerichs I, Guttmann J, Moller K. A lung area estimation method for analysis of ventilation inhomogeneity based on electrical impedance tomography. *J Xray Sci Technol* 2010;18:171-182.

24.   Deibele JM, Luepschen H, Leonhardt S. Dynamic separation of pulmonary and cardiac changes in electrical impedance tomography. *Physiol Meas* 2008;29:S1-14.

25.   Crapo RO, Morris AH, Clayton PD, Nixon CR. Lung volumes in healthy nonsmoking adults. *Bull Eur Physiopathol Respir* 1982;18:419-425.

26.   Woitzik C, Grychtol B, Ferrario D, Böhm S, Robitaille N, Adler A, Alzen G. A priori Informationen für die elektrische Impedanztomografie (EIT) aus CT-daten des Thorax – Erhebung und Bearbeitung anthropometrischer Daten und Konturanalysen unter besonderer Berücksichtigung von pädiatrischen Patienten. *Fortschr Rontgenstr* 2013;185:V28.

27.   Fagerberg A, Stenqvist O, Aneman A. Monitoring pulmonary perfusion by electrical impedance tomography: An evaluation in a pig model. *Acta Anaesthesiol Scand* 2009;53:152-158.

28.   Frerichs I, Pulletz S, Elke G, Reifferscheid F, Schadler D, Scholz J, Weiler N. Assessment of changes in distribution of lung perfusion by electrical impedance tomography. *Respiration* 2009;77:282-291.

29.   Leathard AD, Brown BH, Campbell J, Zhang F, Morice AH, Tayler D. A comparison of ventilatory and cardiac related changes in EIT images of normal human lungs and of lungs with pulmonary emboli. *Physiol Meas* 1994;15 Suppl 2a:A137-146.

30.   Smit HJ, Vonk-Noordegraaf A, Marcus JT, van der Weijden S, Postmus PE, de Vries PM, Boonstra A. Pulmonary vascular responses to hypoxia and hyperoxia in healthy volunteers and COPD patients measured by electrical impedance tomography. *Chest* 2003;123:1803-1809.

31.   Hahn G, Dittmar J, Just A, Quintel M, Hellige G. Different approaches for quantifying ventilation distribution and lung tissue properties by functional EIT. *Physiol Meas* 2010;31:S73-84.

32.   Wilkinson AJ, Randall EW, Cilliers JJ, Durrett DR, Naidoo T, Long T. A 1000-measurement frames/second ERT data capture system with real-time visualization. *IEEE Sens J* 2005;5:300-307.

33.   Yerworth R, Bayford R. The effect of serial data collection on the accuracy of electrical impedance tomography images. *Physiol Meas* 2013;34:659-669.

34.   Gagnon H, Grychtol B, Adler A. A comparison framework for temporal image reconstructions in electrical impedance tomography. *Physiol Meas* 2015;36:1093-1107.

35.   Pulletz S, Kott M, Elke G, Schadler D, Vogt B, Weiler N, Frerichs I. Dynamics of regional lung aeration determined by electrical impedance tomography in patients with acute respiratory distress syndrome. *Multidiscip Respir Med* 2012;7:44.

36.   Bodenstein M, Boehme S, Bierschock S, Vogt A, David M, Markstaller K. Determination of respiratory gas flow by electrical impedance tomography in an animal model of mechanical ventilation. *BMC Pulm Med* 2014;14:73.

37.   Vogt B, Pulletz S, Elke G, Zhao Z, Zabel P, Weiler N, Frerichs I. Spatial and temporal heterogeneity of regional lung ventilation determined by electrical impedance tomography during pulmonary function testing. *J Appl Physiol* 2012;113:1154-1161.

38.   Zhao Z, Muller-Lisse U, Frerichs I, Fischer R, Moller K. Regional airway obstruction in cystic fibrosis determined by electrical impedance tomography in comparison with high resolution CT. *Physiol Meas* 2013;34:N107-114.

39.   Zhao Z, Fischer R, Frerichs I, Muller-Lisse U, Moller K. Regional ventilation in cystic fibrosis measured by electrical impedance tomography. *J Cyst Fibros* 2012;11:412-418.

40.   Frerichs I, Zhao Z, Becher T, Zabel P, Weiler N, Vogt B. Regional lung function determined by electrical impedance tomography during bronchodilator reversibility testing in patients with asthma. *Physiol Meas* 2016;37:698-712.

41.   Vogt B, Zhao Z, Zabel P, Weiler N, Frerichs I. Regional lung response to bronchodilator reversibility testing determined by electrical impedance tomography in chronic obstructive pulmonary disease. *Am J Physiol Lung Cell Mol Physiol* 2016;311:L8-L19.

42.   Zadehkoochak M, Blott BH, Hames TK, George RF. Pulmonary perfusion and ventricular ejection imaging by frequency domain filtering of EIT (electrical impedance tomography) images. *Clin Phys Physiol Meas* 1992;13 Suppl A:191-196.

43.   Smallwood RH, Hampshire AR, Brown BH, Primhak RA, Marven S, Nopp P. A comparison of neonatal and adult lung impedances derived from EIT images. *Physiol Meas* 1999;20:401-413.

44.   Braun F, Proença M, Rapin M, Alba X, Lekadir K, Lemay M, Sola J, Frangi AF, Thiran JP. 4D heart model helps unveiling contributors to cardiac EIT signal. In: Sola J, Braun F, Adler A, editors. 16th International Conference on Biomedical Applications of Electrical Impedance Tomography. Neuchatel; 2015. p. 107.

45.   Nguyen DT, Jin C, Thiagalingam A, McEwan AL. A review on electrical impedance tomography for pulmonary perfusion imaging. *Physiol Meas* 2012;33:695-706.

46.   Fagerberg A, Sondergaard S, Karason S, Aneman A. Electrical impedance tomography and heterogeneity of pulmonary perfusion and ventilation in porcine acute lung injury. *Acta Anaesthesiol Scand* 2009;53:1300-1309.

47.   Frerichs I, Pulletz S, Elke G, Gawelczyk B, Frerichs A, Weiler N. Patient examinations using electrical impedance tomography-sources of interference in the intensive care unit. *Physiol Meas* 2011;32:L1-L10.